

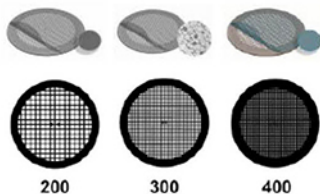
## Nanocharacterization by TEM and AFM

We offer a wide range of TEM and AFM tools, from TEM grids and finders to AFM substrates and grippers.

Available in a wide variety of designs and materials to support your work, select from a broad range of mesh sizes, specimen supporting films, and materials that perfectly suit the conditions of your TEM analysis.

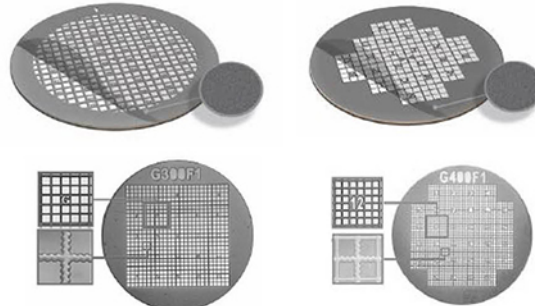
### TEM grid specifications:

Material	Mesh Size and Shape	Film Specifications
<ul style="list-style-type: none"><li>• Cu</li><li>• Ni</li><li>• Au</li><li>• Mo</li><li>• Cu/Pd</li></ul>	<ul style="list-style-type: none"><li>• Square or hexagonal</li><li>• Single-hole grid (75 mm or 100 mm)</li><li>• 100</li><li>• 150</li><li>• 200</li><li>• 300</li><li>• 400</li></ul>	<ul style="list-style-type: none"><li>• None</li><li>• Continuous formvar film (thicknesses: 5-6 nm, 10 nm)</li><li>• Lacey carbon film (average hole sizes: 50 nm, 100 nm, 150 nm, 100 nm, 150 nm)</li><li>• Continuous amorphous carbon film (thicknesses: 10 nm, 20-30 nm)</li><li>• Continuous formvar/carbon film (thickness: 10nm formvar and 1nm carbon)</li></ul>



### TEM finder grid specifications:

Material	Mesh Size	Film Specifications
<ul style="list-style-type: none"><li>• Cu</li><li>• Ni</li><li>• Au</li></ul>	<ul style="list-style-type: none"><li>• 135</li><li>• 200</li><li>• 300</li><li>• 400</li></ul>	<ul style="list-style-type: none"><li>• None</li><li>• Continuous amorphous carbon film (thicknesses: 3-4 nm, 10 nm, 20-30 nm)</li></ul>



### Supporting Tools for Nanomaterial Characterization

Our comprehensive range of supporting materials for nanomaterial characterization includes tweezers (sharp tip, disc gripper for AFM), TEM window grids (various thicknesses, 1 or 9 windows), a magnetic pick-up tool, a grid storage box, cryo-capsules, lift-out grids (Cu or Mo), AFM substrates (various dimensions), and much more.



Explore our complete range of TEM grids on:  
[SigmaAldrich.com/nanocharacterization](https://SigmaAldrich.com/nanocharacterization)

© 2022 Merck KGaA, Darmstadt, Germany and/or its affiliates. All Rights Reserved. Merck, the vibrant M, and Sigma-Aldrich are trademarks of Merck KGaA, Darmstadt, Germany or its affiliates. All other trademarks are the property of their respective owners. Detailed information on trademarks is available via publicly accessible resources.

MK\_AD9792EN 43729 08/2022

The Life Science business of Merck operates as MilliporeSigma in the U.S. and Canada.

**Sigma-Aldrich®**  
Lab & Production Materials

# Leveraging Synergies by Combining Polytetrafluorethylene with Polyvinylidene Fluoride for Solvent-Free Graphite Anode Fabrication

Yang Zhang, Song Lu, Fengliu Lou,\* and Zhixin Yu\*

Solvent-free graphite anode is fabricated successfully with the synergistic effect of polytetrafluorethylene (PTFE) and polyvinylidene fluoride (PVDF). PTFE acts as a processing aid reagent to form a self-supporting electrode film, while PVDF acts as a functional binder when PTFE decomposes in the first lithiation process. The solvent-free graphite electrode with high loading of  $15 \text{ mg cm}^{-2}$  shows good stability with more than 95% capacity retention after 50 charge/discharge cycles under the current of  $0.23 \text{ mA cm}^{-2}$ . Electrodes with extra high loading of  $27 \text{ mg cm}^{-2}$  ( $8.2 \text{ mAh cm}^{-2}$ ) are fabricated and show good stability. Initial coulombic efficiency increases to 89% after prelithiation in the full cell with lithium iron phosphate as cathode. The capacity retention of full cells is more than 80% after 110 cycles under the current of  $0.7 \text{ mA cm}^{-2}$  in coin cells. The roll-to-roll production makes the procedure compatible with current commercial lithium-ion batteries production lines, exhibiting great potential for upscaling production.

## 1. Introduction

The implementation of lithium-ion batteries (LiBs) in electric vehicles (EVs) and stationary grids needs to overcome the bottlenecks of current LiBs, especially low energy density and high cost.<sup>[1–3]</sup> The manufacturing cost and energy density of LiBs are determined to a large extent by electrodes' chemical composition and manufacturing process.<sup>[4,5]</sup> Commercial electrodes are fabricated via the slurry casting (SC) procedure, where active material, binder, and conductive additives are mixed with solvent, typically water for anode, while *N*-methyl-2-pyrrolidone


(NMP) for cathode, to form slurry with appropriate viscosity. The slurry is subsequently cast onto a substrate with aluminum foil for cathode and copper foil for anode and then dried under high temperature followed by pressing with high pressure to get final electrodes. Ovens with dozens of meters are used to evaporate the solvent in a short time. The slurry preparation, coating, and drying account for nearly 50% total energy consumption for LiB production.<sup>[6]</sup> For the cathode side, complicated and expensive NMP recovery is required because it is hazardous to the environment. The high manufacturing cost caused by the SC procedure has no doubt been an obstacle for widespread application of LiBs.

In addition to lowering energy consumption, reducing raw materials is another significant way to reduce the cost of LiBs because they account for  $\approx 60\%$  of the total cost.<sup>[7,8]</sup> Thick electrodes can lower bill of materials (BOM) cost and increase the energy density simultaneously because less auxiliary materials, including current collector, separator, tab and container material, are used for the same specific capacity. For the commercial graphite electrodes, the thickness of the electrode is less than  $100 \mu\text{m}$  with areal capacity of  $2\text{--}3 \text{ mAh cm}^{-2}$ .<sup>[9]</sup> Increasing the areal capacity can drastically increase the energy density of the LiBs because more active materials are deployed within same cell volume. However, defects including electrode cracking, active powder drops, and delamination of active materials from the substrate caused by uneven binder distribution limit the thickness of electrodes fabricated by the SC procedure.<sup>[10–13]</sup> Removing solvent from the electrode fabrication is a promising solution to address the aforementioned issues.

Tremendous efforts are being dedicated to solvent-free (SF) technology for electrode fabrication. Vapor deposition is utilized for SF thin electrode fabrication, where raw materials are vaporized and deposited onto the substrate. Vapor deposition includes magnetron sputtering, thermal evaporation, pulsed laser deposition, atomic layer deposition, etc. Kuwata et al. fabricated solid-state-thin-film batteries consisting of  $\text{Li}_2\text{O-V}_2\text{O}_5\text{-SiO}_2$  solid electrolyte (SE),  $\text{LiCoO}_2$  (LCO) cathode, and  $\text{SnO}$  anode using pulsed laser deposition technology, where the laser beam was focused onto the rotating target under vacuum.<sup>[14]</sup> Shiraki et al. controlled the crystal orientation of LCO with a similar procedure to obtain the most appropriate orientation for ion conduction.<sup>[15]</sup> Epitaxial LCO thin films with polycrystalline  $\text{Li}_{1.2}\text{CoO}_2$  as target were deposited with a thickness of  $200 \text{ nm}$ . The films were

Y. Zhang, S. Lu, Z. Yu  
Department of Energy and Petroleum Engineering  
University of Stavanger  
4036 Stavanger, Norway  
E-mail: zhixin.yu@uis.no

Y. Zhang, F. Lou  
Beyond AS  
4313 Sandnes, Norway  
E-mail: fengliu@beyond.no

 The ORCID identification number(s) for the author(s) of this article can be found under <https://doi.org/10.1002/ente.202200732>.

© 2022 The Authors. Energy Technology published by Wiley-VCH GmbH. This is an open access article under the terms of the Creative Commons Attribution-NonCommercial License, which permits use, distribution and reproduction in any medium, provided the original work is properly cited and is not used for commercial purposes.

DOI: 10.1002/ente.202200732

subsequently annealed at 650 °C in air to obtain final LCO electrodes. Ionized magnetron sputter deposition can be applied with a relatively low temperature of 350 °C.<sup>[16]</sup> The thin-film batteries prepared by vapor deposition exhibited good performance, such as high energy density,<sup>[17,18]</sup> long cycling life,<sup>[19]</sup> and improved rate capability.<sup>[20,21]</sup> However, vapor deposition technology is only suitable for the fabrication of electrode with small size, mainly for microelectronic devices and highly integrated circuits. The expensive equipment and complicated film-forming process, high energy consumption, and low areal capacity limit its application in EVs or even 3C consumer electronics. Extrusion can be used for SF electrode fabrication with extra high thickness. Sotomayor et al. were the first to use extrusion as an SF method to fabricate electrode with lithium titanate oxide (LTO) and lithium iron phosphate (LFP) as active materials.<sup>[22]</sup> This process comprises particle mixing, extrusion, debinding, and sintering. A blend of polypropylene, paraffin wax, and stearic acid was used as the sacrificial binder. A double-heating step in *n*-heptane was required to degrade the polymers, and high temperature was applied to sinter electrode. The LFP/LTO cells with areal capacity of 13.3 mAh cm<sup>-2</sup> were fabricated and demonstrated good cycling stability. Melting and extrusion is a scalable procedure for electrode manufacturing with high loading. However, extrusion is sensitive to the particle size and needs accurate control of temperature, shear force, and time of extrusion.<sup>[23]</sup> In addition, high consumption of polymers, a tedious manufacturing procedure, and high temperatures required for debinding and sintering processes impede its further application in practical electrode manufacturing.

Another promising procedure for SF electrode fabrication is using fibrillizable PTFE binder to replace conventional soluble binder. Dry mixing, fibrillation of PTFE, self-supporting electrode film formation, and lamination are involved in this procedure. Maxwell Technology developed this procedure for activated carbon electrodes used for supercapacitors.<sup>[24,25]</sup> Hippauf et al. applied this scalable SF procedure for lithium nickel cobalt manganese oxide (NCM) electrode fabrication in all-solid-state batteries (ASSBs).<sup>[26]</sup> PTFE powder was first mixed and sheared with NCM, SE, and carbon nanofiber (CNF) in a mortar for one minute until the formation of single flake. The flake was subsequently hot rolled several times to desired thickness. The content of PTFE can be reduced to 0.1 wt%, which is beneficial for ion transport. The pouch cell showed decent cycling stability with 93.2% capacity retention after 100 cycles under the current of 0.7 mA cm<sup>-2</sup>. Zhou et al. successfully scaled up this procedure to pilot stage for fabrication of LFP electrodes, where high-speed air blowing, hot rolling, and hot overlying process were adopted.<sup>[27]</sup> The jet mill with high-pressure dry air was used to extend PTFE molecular chain. Cotton candy-like mixture was formed, and the mixture was hot rolled twice at 180 °C to form a free-standing electrode film using a horizontal-type roller. The LFP cathode was fabricated with compact densities, almost 1.6 times higher than SC electrodes. 40% activated carbon was required to increase the flexibility of the LFP electrodes.

The lowest unoccupied molecular orbital (LUMO) of PTFE is low, making it easy to accept electrons and get reduced when used in anodes.<sup>[28–30]</sup> The instability issue of PTFE in SF anode fabrication is still a challenge. In our previous work, we successfully fabricated SF hard carbon/soft carbon anode with the

fibrillation of PTFE.<sup>[31]</sup> The SF hard carbon anodes demonstrated comparable cycling life with their SC counterparts, even though most PTFE fibrils were reduced at the first lithiation process. However, SF graphite anode exhibited fast capacity fading. The disappearance of PTFE peak from 19° in X-Ray diffraction (XRD) demonstrated fast capacity fading resulting from the decomposition of PTFE. To expand the application of this procedure to other anode active materials like graphite with big volume variation during the charge/discharge process, PVDF has been reported to be promising to address the instability issue caused by the reduction of PTFE.

In this study, we successfully expanded PTFE for graphite anode fabrication with the help of PVDF. The thick SF graphite anode (180 μm) could be easily fabricated, which could significantly increase the specific energy of LiB cell. The SF graphite anode demonstrated good stability under high loading. The good electrochemical performance and compatibility with the roll-to-roll production line enable the SF procedure potentially to replace current commercial SC procedures.

## 2. Experimental Section

### 2.1. Dry-Mixing Optimization

A conical mixer (Figure S1, Supporting Information, Xinyang, Wuxi, China) was used for dry mixing. Graphite (CP5H, Shanshan, Shanghai, China) and carbon black were baked at 150 °C overnight before mixing. Graphite, carbon black, and PVDF (HSV900, Arkema, Colombes Cedex, France) were mixed with a mass ratio of 90:5:2. The mixing time and speed were screened to get optimal mixing parameters.

### 2.2. Electrode Fabrication

**Figure 1** shows the schematic process of SF PVDF graphite anode fabrication combining PTFE and PVDF. Graphite, PVDF, carbon black, and PTFE powder (MTI, Shenzhen, China) were used directly for anode fabrication. A powder mixture was prepared by mixing graphite, carbon black, and PVDF in a conical mixer at a speed of 1200 r min<sup>-1</sup> for 90 min. After that, PTFE powder was added to the mixture and mixed for 30 min using a V blender. The high-speed dry air was then applied using 2 in. grinding chamber jet mill (Sturtevant, Hanover, NC, US) to fibrillate PTFE to a cotton candy-like dry mixture. The weight ratio of graphite/carbon black/PVDF/PTFE was 90/5/2/3. For comparison, graphite anode without PVDF was also fabricated by a similar procedure with the weight ratio of 90/5/5 (graphite/carbon black/PTFE). The free-standing electrode film was formed when the dry mixture was hot rolled at 160 °C using a calendar machine at a speed of 15 cm min<sup>-1</sup>. The thickness of the electrode film was adjusted according to the gap between the rolls of the calendar machine. The electrode film could be folded several times without any obvious cracks or defects, indicating good flexibility and mechanical strength, which are critical for upscaling production. Finally, the free-standing film was laminated to the carbon-coated copper foil using hot rolling at 80 °C before the electrode film was baked at 180 °C for 10 min. For convenience, SF graphite anode with PVDF will be denoted as SF

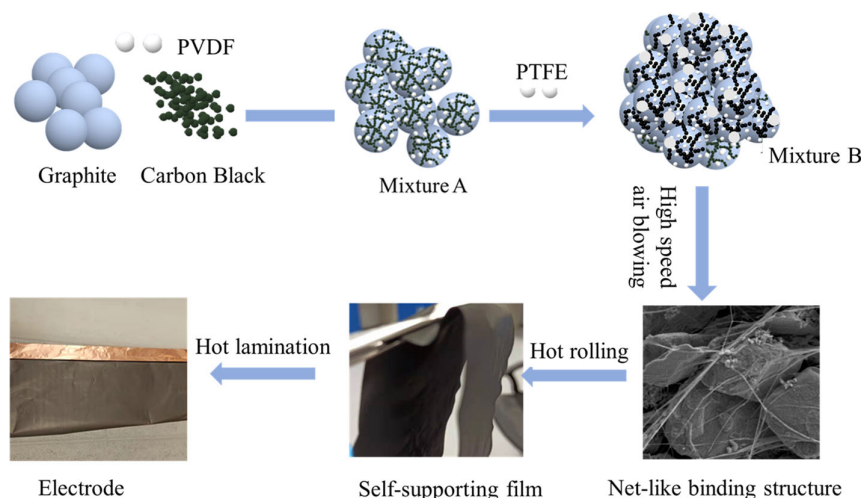


**Figure 1.** Schematic process diagram of SF PVDF graphite electrode fabrication based on PTFE fibrillation, including dry mixing, fibrillation, hot rolling, and lamination.

PVDF graphite anode, while SF graphite anode without PVDF will be denoted as SF graphite anode. For PTFE film fabrication, 80% carbon black was added to increase the electrical conductivity: the PTFE powder and carbon black were mixed for 30 min in a kitchen mixer and then the mixture was ground in a agate mortar until the formation of flake; finally, the flask was hot rolled using a calendar machine.

### 2.3. Cell Assembly

Both half cells and full cells were assembled with 2032 coin cell parts (MTI, Shenzhen, China) in an argon-filled glovebox, where water and oxygen concentrations were less than 0.01 ppm. Cellulose film (Celgard, Charlotte, NC, US), lithium foil (Sigma-Aldrich, 600  $\mu\text{m}$ , Darmstadt, Germany), and 50  $\mu\text{L}$  1.2 M  $\text{LiPF}_6$  in EC-EMC (3/7, v/v) with 10 wt% fluoroethylene carbonate (FEC) were used as the separator, encounter electrode, and electrolyte, respectively. For full cell assembly, commercial lithium iron phosphate (LFP) electrodes from Beyonder AS (Norway) were used as cathode. The capacity ratio of anode (NP ratio) to cathode was 1.1:1.

### 2.4. Prelithiation

Single-layer pouch cell was assembled with the commercial LFP electrode as cathode, SF graphite electrode as anode, and single polyethylene (PE) as separator, respectively. Commercial electrolyte (Tianci, Wuxi, China) was used directly. The pouch cell was aged for 12 h before charging to a certain state of charge (SOC). Thereafter, the cells were disassembled in a glovebox and the lithiated SF graphite anodes were washed with dimethyl carbonate (DMC) several times and dried under room temperature for full cell assembly.

### 2.5. Electrochemical and Morphological Characterization

The galvanostatic charge/discharge tests were performed under room temperature using an eight-channel battery analyzer

(Neware, Shenzhen, China). The voltage ranges were 0.01–1.5 V and 2.5–3.65 V for half cells and full cells, respectively. All cells were aged under room temperature for 12 h before testing and underwent several formation cycles. Cyclic voltammetry (CV) was carried out in the voltage range of 0.01–3.2 V at a scanning rate of 0.5  $\text{mV s}^{-1}$ .

The pristine and cycled electrodes were characterized using a scanning electron microscope (SEM, Phenomenon LE). The cycled electrodes were charged to the full delithiation state after cell cycling, followed by disassembling the cell, dipping the electrode into DMC solution for 2 h to remove any residual electrolyte, and drying at room temperature overnight in an argon-filled glovebox for further ex situ analysis.

## 3. Results and Discussion

To study the stability of PTFE at anode, PTFE film with 80% carbon black was prepared. The film was used directly without current collector to assemble coin cells with lithium foil as the counter electrode. The charge/discharge cycling test was conducted under a current of 1.2  $\text{mA cm}^{-2}$ . As shown in **Figure 2a**, the capacity–voltage curves showed that PTFE delivered a capacity of 970  $\text{mAh g}^{-1}$  at the first lithiation process, while the capacity of the first delithiation reduced to less than 20  $\text{mAh g}^{-1}$ , demonstrating the irreversible reduction of PTFE during the first lithiation process. The lithiation and delithiation capacity in the second cycle is 191 and 97  $\text{mAh g}^{-1}$ , respectively. The lithiation capacity in the second cycle is more than the delithiation capacity, which could be attributed to the reaction of PTFE with lithium ion in the lithiation process, because not all PTFE is reduced in the previous lithiation process. CV curves (**Figure 2b**) demonstrated that a reduction peak appeared at  $\approx 1$  V in the first reduction cycle, which could be ascribed to the irreversible reaction of PTFE and lithium ion. The reduction peak became weaker in the following cycles, demonstrating that most PTFE was reduced in the first lithiation process. The CV result is consistent with charge/discharge cycling testing and earlier studies.<sup>[28]</sup> SEM was used to characterize the morphology of both pristine

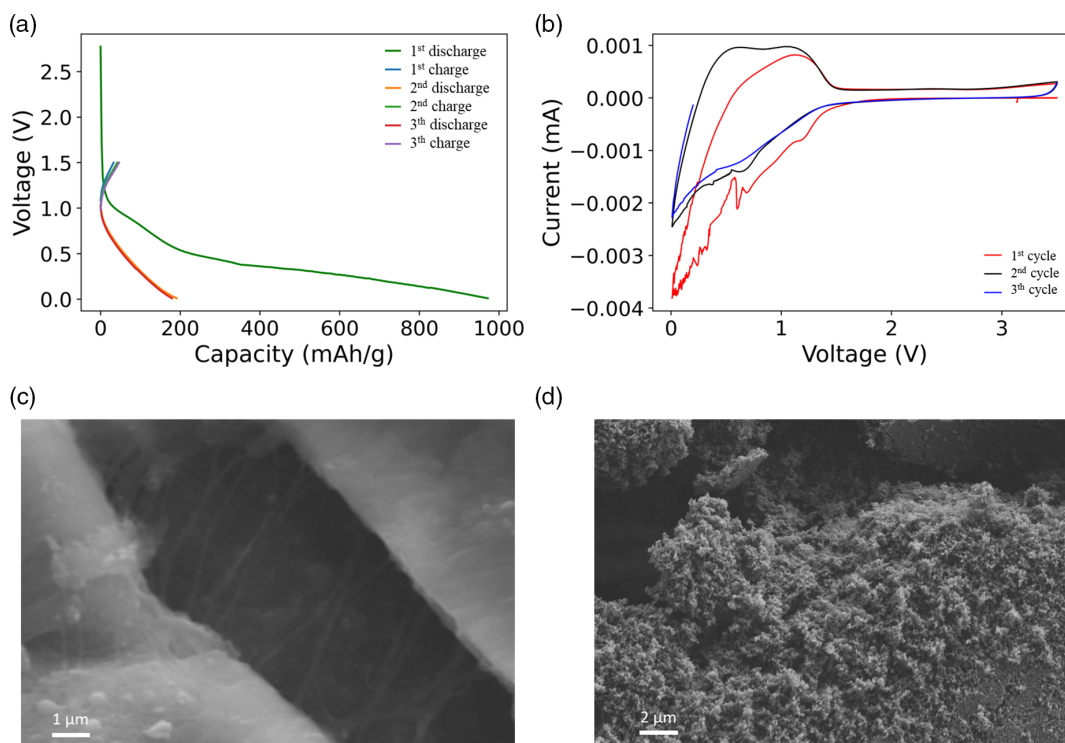


**Figure 2.** Stability analysis of PTFE at anode: a) capacity–voltage curves for PTFE film with 20% carbon black; b) CV curves of PTFE film; c) SEM image of the pristine PTFE film; and d) SEM image of PTFE film after lithiation.

PTFE film and PTFE film after lithiation. The PTFE fibrils are apparent from the pristine PTFE film (Figure 2c), while most of PTFE fibrils disappeared after lithiation (Figure 2d). SEM characterization further proved the irreversible reduction of PTFE during the first lithiation process.

In the dry-mixing process, materials with different densities and sizes tend to agglomerate, which is detrimental to the electrical conductivity of electrodes and rate capability. Mixing parameters like mixing time and speed were screened and optimized. The dry mixture powder mixed under different speeds and times were hot rolled under 120 °C several times to get an electrode film with a thickness of 100 μm. The ohmic resistances of electrode films obtained under different mixing conditions are shown in Table 1. Surprisingly, the electrical conductivity did not increase with mixing time or mixing speed. For instance, with a fixed speed of 1200 r min<sup>-1</sup>, the resistance decreased from 1.831 to 1.412 mΩ when increasing the mixing time from 30 to 90 min. The resistance didn't decrease with

**Table 1.** Ohmic resistance of mixture A under different dry mixing times and speeds (mΩ).

Mixing speed	30 min	60 min	90 min	120 min
400 [r min <sup>-1</sup> ]	3.766	3.125	2.785	2.042
800 [r min <sup>-1</sup> ]	2.015	1.827	1.679	1.594
1200 [r min <sup>-1</sup> ]	1.831	1.654	1.412	1.422
1400 [r min <sup>-1</sup> ]	1.733	1.615	1.448	1.437

prolonged mixing time. The best conductivity was obtained after 90 min mixing under 1200 r min<sup>-1</sup> mixing speed.

To increase the adhesion between the current collector and electrode film, 10 μm copper foil with primer was used as the current collector. Slurry with poly(ethylene oxide) (PEO)/carbon black mass ratio of 50/50 was prepared and cast onto Cu foil using a doctor blade. The final primer thickness is 1 μm, which has negligible effects on the energy density of electrodes. The uniform distribution of carbon black on the surface of copper foil is shown in Figure S2, Supporting Information, which makes the primer-coated current collector have comparable electroconductivity to bare copper foil. Hot rolling was deployed for the lamination of the electrode film and primer-coated Cu foil. The lamination temperature was screened from 40 to 160 °C. The maximum adhesion was obtained at 80 °C. The adhesion increased from 2.3 to 6.8 N m<sup>-1</sup> when the lamination temperature increased from 40 to 80 °C. The adhesion has negligible variation when the lamination temperature further increased. The improved adhesion with increasing temperature from 40 to 80 °C is ascribed to the melting of PEO, since PEO has melting point of about 70 °C. When the lamination temperature exceeds the melting point, PEO will have more contact area with the electrode film. However, further increasing the temperature above the melting point cannot increase contact area, exhibiting little impact on adhesion strength.

SEM was also used to analyze the morphology of the pristine SF PVDF graphite anodes. The carbon black is distributed on the surface of graphite particles without obvious agglomeration, clarifying sufficient mixing of graphite and conductive additives

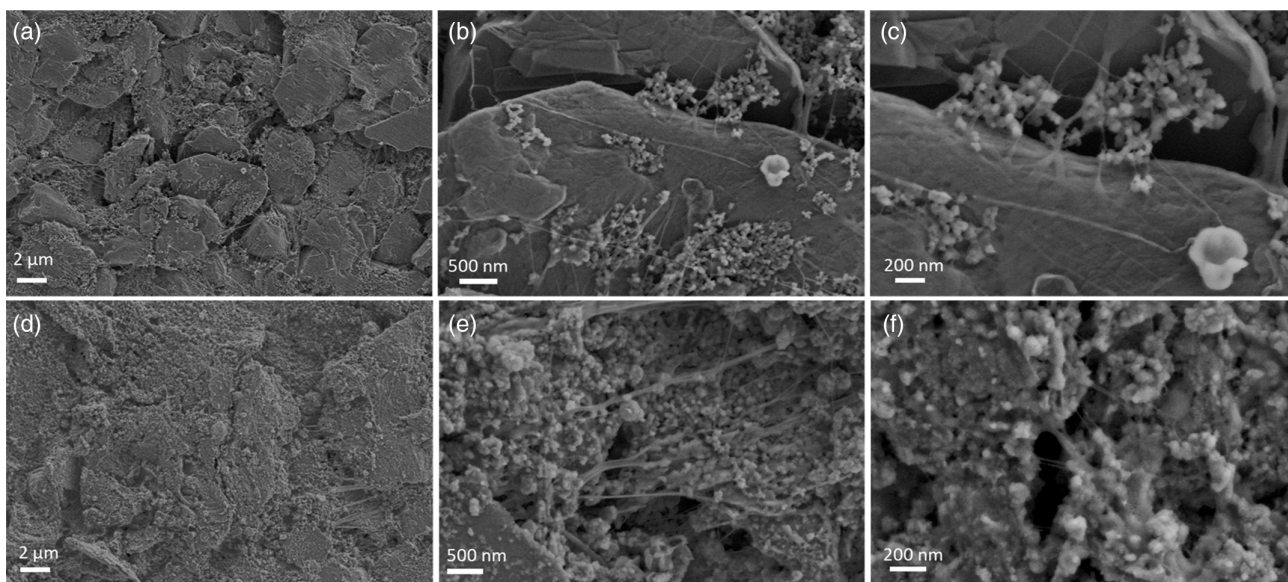


**Figure 3.** Top-view SEM images of pristine SF graphite anodes with different magnifications: a) 10 000 $\times$ , b) 50 000 $\times$ , and c) 100 000 $\times$ ; SF graphite anodes after 100 cycles with different magnifications: d) 10 000 $\times$ , e) 50 000 $\times$ , and f) 100 000 $\times$ .

(Figure 3a). No PVDF particles were observed, showing that most PVDF was melted around the surface of graphite particles. The PTFE fibrils could be observed (Figure 3a–c), which bundle with graphite to form a net-like structure, ensuring good mechanical strength of the film with a tensile strength of  $7.8 \text{ N m}^{-1}$  ( $100 \mu\text{m}$ ) and good flexibility (Figure 1, self-supporting film). The PTFE distributes evenly among the electrode, which was confirmed by the cross-sectional SEM images (Figure 4a–c). SEM–energy dispersive X-ray spectroscopy (EDS) mapping of the pristine SF PVDF graphite electrode further confirmed that fluorine is uniformly distributed on the surface of the electrode

(Figure 5). The SF graphite anodes without PVDF showed similar morphology (Figure S3a–c, Supporting Information).

The cycling stability of SF PVDF graphite anode was studied in half cells with a current of  $0.23 \text{ mA cm}^{-2}$  at room temperature. In contrast to fast capacity fading of SF graphite electrode (without PVDF) in our previous study,<sup>[31]</sup> the capacity retention for SF PVDF graphite anode was more than 95% after 50 charge/discharge cycles with high areal capacity of  $4.22 \text{ mAh cm}^{-2}$ , as shown in Figure 6a. The low initial coulombic efficiency (ICE) of 85.6% is the result of the irreversible reaction between PTFE and active lithium ion (Figure 6b). The coulombic

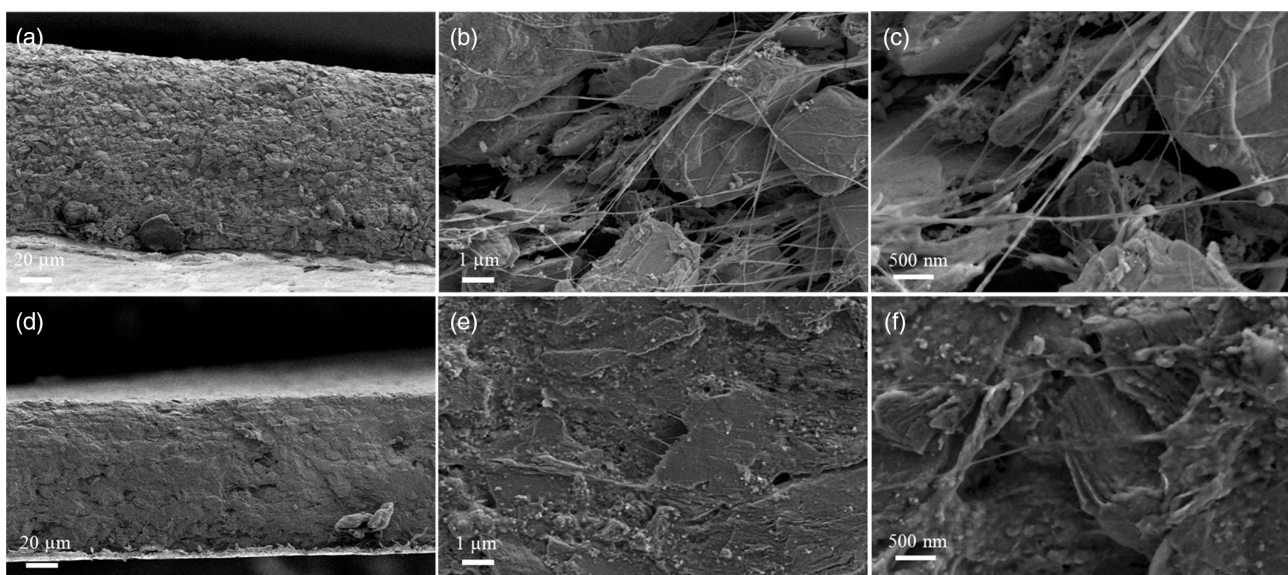


**Figure 4.** Cross-sectional SEM images of pristine SF PVDF graphite anodes with different magnifications: a) 1000 $\times$ , b) 20 000 $\times$ , and c) 50 000 $\times$ ; SF PVDF graphite anodes after 100 cycles with different magnifications: d) 1000 $\times$ , e) 20 000 $\times$ , and f) 50 000 $\times$ .

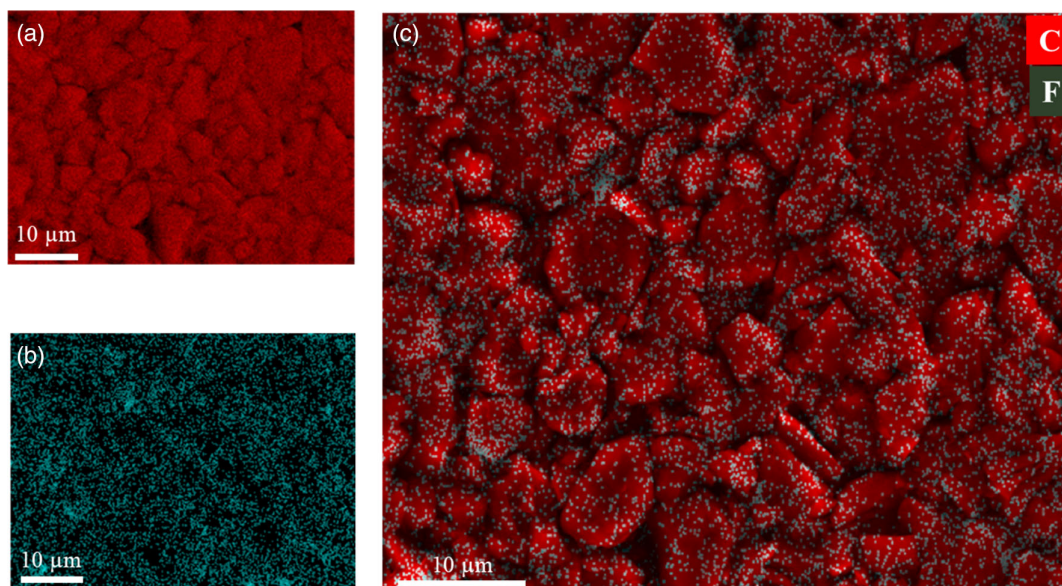


**Figure 5.** SEM–EDS mapping of fresh SF PVDF graphite anode (Graphite: Carbon black: PTFE: PVDF = 90: 5: 3: 2). a) carbon distribution; b) fluorine distribution; and c) overlay of carbon and fluorine distribution.

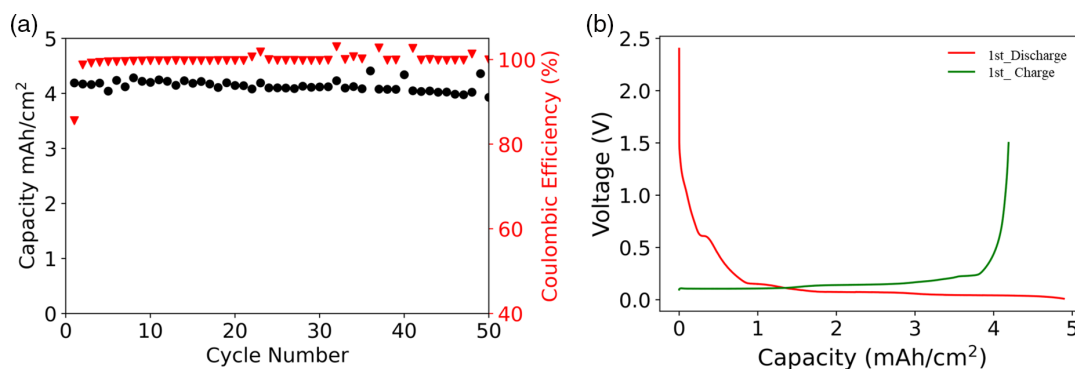


**Figure 6.** a) Cycling performance of SF graphite anode at the current of  $0.23 \text{ mA cm}^{-2}$  and room temperature; b) voltage–capacity curves of SF graphite anode for the first lithiation and delithiation process.

efficiency (CE) increased to more than 99% from second cycle, indicating that most PTFE was reduced in the first cycle. The CE further increased to 99.7% at 10th cycle and was stable after the 10th cycle, proving the stability of SF PVDF graphite anode (Figure 6a).

The morphology of the cycled SF PVDF graphite electrodes was also studied to explore the stability mechanism, taking into consideration that most PTFE degraded. As shown in Figure S3d,e, Supporting Information, apparent cracks could be observed from the top view of the cycled SF graphite anodes (without PVDF). There were almost no fibrils left (Figure S3f, Supporting Information). Graphite has roughly 10% volume swelling and shrinking during the lithiation and delithiation process.<sup>[32,33]</sup> The reduction of PTFE makes the electrode unable to accommodate the volume variation and the electrode loses integrity, resulting in very fast capacity fading. However, no apparent cracks were observed from the top view of SF PVDF graphite anode after 100 charge/discharge cycles (Figure 3d–f). EDS

mapping also showed even distribution of fluorine after 100 cycles (Figure S4, Supporting Information). The cross-sectional SEM images of cycled SF PVDF graphite anode (Figure 4d–f) further demonstrated that the electrodes maintain compact structure as good as the pristine one (Figure 4a–c), even though most PTFE fibrils were reduced. No obvious separation between the electrode film and the current collector was observed (Figure 4d), indicating good adhesion between the electrode film and the primer-coated current collector. Therefore, it could be proposed that the good stability of SF PVDF graphite anode was due to that PTFE acts as a processing acid reagent in SF PVDF graphite anode, while PVDF acts as a functional binder when PTFE is reduced in the first lithiation process.

In addition to energy saving, another big advantage of the SF procedure is the deployment of the thick electrode. We have previously fabricated SF PVDF electrode with areal capacity of more than  $4.2 \text{ mAh cm}^{-2}$  with excellent stability during the cycling test. We further increased the graphite loading to  $27 \text{ mg cm}^{-2}$

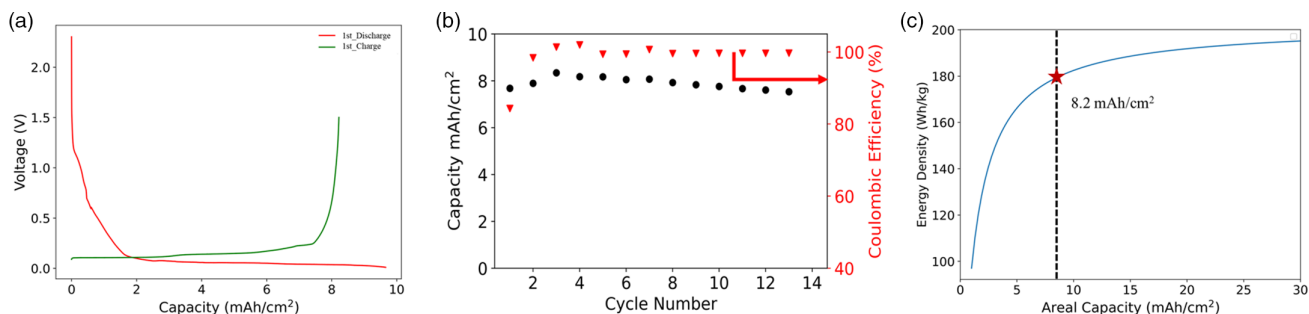


**Figure 7.** a) Voltage–capacity curves for the first lithiation and delithiation process; b) cycling of SF graphite with high loading of  $27 \text{ mg cm}^{-2}$  and  $180 \mu\text{m}$  under the current of  $0.3 \text{ mA cm}^{-2}$ ; and c) specific energy as a function of areal capacity of graphite anode (parameters used in the calculation are listed in Table S1, Supporting Information).

with a thickness of  $180 \mu\text{m}$  ( $1.67 \text{ g cm}^{-3}$ , 24% porosity). The high loading electrodes delivered an impressive areal capacity of  $8.2 \text{ mAh cm}^{-2}$  (Figure 7a). The areal capacity of SF PVDF graphite anode in our study is not only much higher than commercial graphite electrodes, but also higher than many silicon-based anodes reported in the literature.<sup>[34–37]</sup> The electrodes were stable without obvious capacity fading for 15 cycles under a current density of  $0.3 \text{ mA cm}^{-2}$  (Figure 7b). However, the internal short circuit occurred afterwards, which could be ascribed to the high pressure in coin cells resulting from the thick electrode.

To explore the potential application of our extra high loading electrode for high-energy-density LiBs, the specific energy of LFP/graphite cells was calculated as a function of the areal capacity loading of the graphite anode (Figure 7c). The N/P ratio (capacity of anode/capacity of cathode) was set to 1.1, and the amount of electrolyte was determined with injection coefficient of 3.5 (weight of electrolyte (g)/capacity of cell (Ah)), which is an average value for the commercial LFP/graphite prismatic cells. The detailed calculation method was clarified by Equation (1) in SI. It is worth emphasizing that the weight of packing materials was ignored intentionally because it varies a lot along the cell configuration. Hence the specific energy in our calculation will be slightly higher than the actual value. Figure 7c shows that the energy density of LFP/graphite cells increases fast with the enhancement of areal capacity of graphite anodes when the areal capacity is less than  $10 \text{ mAh cm}^{-2}$ . However, the energy density increase becomes flat with further increase in the areal capacity.

The irreversible reduction of PTFE in the first lithiation process could result in low ICE in full cells. The theoretical irreversible lithiation capacity is  $\approx 1000 \text{ mAh g}^{-1}$ . In our study, 2% of PTFE was used, which will reduce the capacity to  $20 \text{ mAh}$  per gram of electrode. The specific capacity of commercial graphite is around  $350 \text{ mAh g}^{-1}$ . 6% energy density will be lost due to the utilization of 2% PTFE. Therefore, prelithiation is an effective method to compensate lithium consumption caused by the reaction of PTFE and lithium ion. The ICE as well as cycling life can also be improved by the addition of extra lithium inventory. Prelithiation was conducted with a similar procedure as reported in our previous work.<sup>[31]</sup> The pouch cell was charged to  $2.7 \text{ V}$  with the capacity of  $1.1 \text{ mAh cm}^{-2}$  (Figure S5a, Supporting Information). The full cell with LFP cathode was assembled with capacity ratio of anode to cathode (N/P ratio) at 1.1:1. The ICE

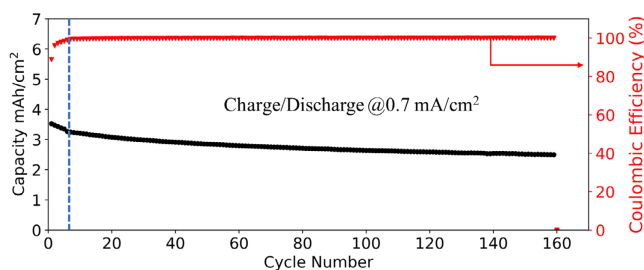


**Figure 8.** Cycling of the prelithiated SF PVDF graphite with LFP as cathode under the current of  $0.7 \text{ mA cm}^{-2}$ .

increased to 89% in full cells (Figure S5b, Supporting Information), which is at similar level as the commercial cells. It's worth noting that the ICE could be further increased by the adjustment of the depth of prelithiation. The prelithiated SF graphite anodes with PVDF showed good stability with about 80% discharge capacity retention after 110 cycles under a current of  $0.7 \text{ mA cm}^{-2}$  (Figure 8). The CE increased to 99.5% and 99.7% and maintained stability after cycles 10 and 20, respectively.

## 4. Conclusions

We successfully expanded PTFE for SF graphite anodes fabrication with synergistic effect of PVDF as the dual binder. Thanks to the binding capability of PVDF, the electrodes were able to keep their integrity even though most PTFE was reduced in first lithiation process. The electrode shows good stability with high loading of  $15 \text{ mg cm}^{-2}$  and more than 95% capacity retention after 50 cycles. The electrodes with extra high loading could be easily prepared, which could lower the manufacturing cost while increase the energy density simultaneously. Furthermore, the method can be conveniently implemented on the existing commercial roll-to roll production line, demonstrating high potential for large-scale production.

## Supporting Information

Supporting Information is available from the Wiley Online Library or from the author.



## Acknowledgements

The authors would like to thank the Norwegian Research Council and Beyond AS for the financial support of this project under project No.310353.

## Conflict of Interest

The authors declare no conflict of interest.

## Author Contributions

Y.Z., S.L., F.L. and Z.Y.: Conceptualization; Y.Z., S.L. and Z.Y.: investigation; Y.Z.: writing-original draft preparation; S.L., F.L. and Z.Y.: writing-review and editing; Y.Z.: funding acquisition; F.L. and Z.Y.: supervision. All authors have read and agreed to the published version of the manuscript.

## Data Availability Statement

The data that support the findings of this study are available from the corresponding author upon reasonable request.

## Keywords

graphite anodes, PTFE, PVDF, solvent free electrodes, synergistic effects

Received: July 7, 2022

Revised: August 8, 2022

Published online: September 1, 2022

- [1] D. Bresser, S. Passerini, B. Scrosati, *Energy Environ. Sci.* **2016**, *9*, 3348.
- [2] J. B. Goodenough, K.-S. Park, *J. Am. Chem. Soc.* **2013**, *135*, 1167.
- [3] M. M. Thackeray, C. Wolverton, E. D. Isaacs, *Energy Environ. Sci.* **2012**, *5*, 7854.
- [4] G. Patry, A. Romagny, S. Martinet, D. Froelich, *Energy Sci. Eng.* **2014**, *3*, 71.
- [5] J. Kasemchainan, P. G. Bruce, *Johnson Matthey Technol. Rev.* **2018**, *62*, 177.
- [6] K.-H. Pettinger, W. Dong, *J. Electrochem. Soc.* **2016**, *164*, A6274.
- [7] G. Berckmans, M. Messagie, J. Smekens, N. Omar, L. Vanhaverbeke, J. Van Mierlo, *Energies* **2017**, *10*, 1314.
- [8] J. W. Choi, D. Aurbach, *Nat. Rev. Mater.* **2016**, *1*, 1.
- [9] S. N. Bryntesen, A. H. Strømman, I. Tolstorebrov, P. R. Shearing, J. J. Lamb, O. Stokke Burheim, *Energies* **2021**, *14*, 1406.
- [10] M. Stein, A. Mistry, P. P. Mukherjee, *J. Electrochem. Soc.* **2017**, *164*, A1616.
- [11] K. Rollag, D. Juarez-Robles, Z. Du, D. L. Wood III, P. P. Mukherjee, *ACS Appl. Energy Mater.* **2019**, *2*, 4464.
- [12] F. Font, B. Protas, G. Richardson, J. M. Foster, *J. Power Sources* **2018**, *393*, 177.
- [13] J. Kumberg, M. Müller, R. Diehm, S. Spiegel, C. Wachsmann, W. Bauer, P. Scharfer, W. Schabel, *Energy Technol.* **2019**, *7*, 1900722.
- [14] N. Kuwata, J. Kawamura, K. Toribami, T. Hattori, N. Sata, *Electrochem. Commun.* **2004**, *6*, 417.
- [15] S. Shiraki, H. Oki, Y. Takagi, T. Suzuki, A. Kumatani, R. Shimizu, M. Haruta, T. Ohsawa, Y. Sato, Y. Ikuhara, *J. Power Sources* **2014**, *267*, 881.
- [16] K.-F. Chiu, *Thin Solid Films* **2007**, *515*, 4614.
- [17] G. Yang, C. Abraham, Y. Ma, M. Lee, E. Helfrick, D. Oh, D. Lee, *Appl. Sci.* **2020**, *10*, 4727.
- [18] A. Patil, V. Patil, D. W. Shin, J.-W. Choi, D.-S. Paik, S.-J. Yoon, *Mater. Res. Bull.* **2008**, *43*, 1913.
- [19] J. Bates, N. Dudney, B. Neudecker, A. Ueda, C. Evans, *Solid State Ionics* **2000**, *135*, 33.
- [20] J. Lin, L. Lin, S. Qu, D. Deng, Y. Wu, X. Yan, Q. Xie, L. Wang, D. Peng, *Energy Environ. Mater.* **2022**, *5*, 133.
- [21] A. Reyes Jiménez, R. Klöpsch, R. Wagner, U. C. Rodehorst, M. Kolek, R. Nölle, M. Winter, T. Placke, *ACS Nano* **2017**, *11*, 4731.
- [22] M. E. Sotomayor, C. de La Torre-Gamarra, B. Levenfeld, J.-Y. Sanchez, A. Varez, G.-T. Kim, A. Varzi, S. Passerini, *J. Power Sources* **2019**, *437*, 226923.
- [23] N. Verdier, G. Foran, D. Lepage, A. Prébé, D. Aymé-Perrot, M. Dollé, *Polymers* **2021**, *13*, 323.
- [24] P. Mitchell, L. Zhong, X. Xi, Recyclable dry particle based adhesive electrode and methods of making same, Google Patents, **2008**.
- [25] P. Mitchell, X. Xi, B. Zou, L. Zhong, Dry particle packaging systems and methods of making same, Google Patents, **2006**.
- [26] F. Hippauf, B. Schumm, S. Doerfler, H. Althues, S. Fujiki, T. Shiratsuchi, T. Tsujimura, Y. Aihara, S. Kaskel, *Energy Storage Mater.* **2019**, *21*, 390.
- [27] H. Zhou, M. Liu, H. Gao, D. Hou, C. Yu, C. Liu, D. Zhang, J.-C. Wu, J. Yang, D. Chen, *J. Power Sources* **2020**, *473*, 228553.
- [28] G. Li, R. Xue, L. Chen, *Solid State Ionics* **1996**, *90*, 221.
- [29] R. J. Brodd, A. Kozawa, M. Yoshio, *Lithium-Ion Batteries: Science and Technologies*, Springer, Berlin **2009**.
- [30] Q. Wu, J. P. Zheng, M. Hendrickson, E. J. Plichta, *MRS Adv.* **2019**, *4*, 857.
- [31] Y. Zhang, F. Huld, S. Lu, C. Jektvik, F. Lou, Z. Yu, *Batteries* **2022**, *8*, 57.
- [32] L. Mickelson, H. Castro, E. Switzer, C. Friesen, *J. Electrochem. Soc.* **2014**, *161*, A2121.
- [33] T. Ohzuku, N. Matoba, K. Sawai, *J. Power Sources* **2001**, *97*, 73.
- [34] P. Li, J. Hwang, Y. Sun, *ACS Nano* **2019**, *13*, 2624.
- [35] T. He, J. Feng, Y. Zhang, L. Zu, G. Wang, Y. Yu, J. Yang, *Adv. Energy Mater.* **2018**, *8*, 1702805.
- [36] M.-G. Jeong, H. L. Du, M. Islam, J. K. Lee, Y.-K. Sun, H.-G. Jung, *Nano Lett.* **2017**, *17*, 5600.
- [37] M. Ko, S. Chae, J. Ma, N. Kim, H.-W. Lee, Y. Cui, J. Cho, *Nat. Energy* **2016**, *1*, 1.